

Western University

Scholarship@Western

---

Chemical and Biochemical Engineering  
Publications

Chemical and Biochemical Engineering  
Department

---

12-6-2022

## Controlling Differentiation of Adult Stem Cells Via Cell-Derived Nanoparticles: Implications in Bone Repair

Shruthi Polla Ravi  
*Western University*

Yasmeen Shamiya  
*Western University, yshamiya@uwo.ca*


Aishik Chakraborty  
*Western University, achakr26@uwo.ca*

Ali Coyle  
*Western University*

Alap A. Zahid  
*Western University, AZAHID25@uwo.ca*

*See next page for additional authors*

Follow this and additional works at: <https://ir.lib.uwo.ca/chemengpub>

 Part of the [Biomedical Engineering and Bioengineering Commons](#), and the [Chemical Engineering Commons](#)

---

### Citation of this paper:

Ravi, Shruthi Polla; Shamiya, Yasmeen; Chakraborty, Aishik; Coyle, Ali; Zahid, Alap A.; Wang, Jin; Boutilier, Michael; Ho, Emmanuel; and Paul, Arghya, "Controlling Differentiation of Adult Stem Cells Via Cell-Derived Nanoparticles: Implications in Bone Repair" (2022). *Chemical and Biochemical Engineering Publications*. 9.

<https://ir.lib.uwo.ca/chemengpub/9>

---

**Authors**

Shruthi Polla Ravi, Yasmeen Shamiya, Aishik Chakraborty, Ali Coyle, Alap A. Zahid, Jin Wang, Michael Boutilier, Emmanuel Ho, and Arghya Paul

# **Controlling Differentiation of Adult Stem Cells *via* Cell-derived Nanoparticles: Implications in Bone Repair**

*Shruthi Polla Ravi*<sup>a</sup>, *Yasmeen Shamiya*<sup>b</sup>, *Aishik Chakraborty*<sup>c</sup>, *Ali Coyle*<sup>a</sup>, *Alap Ali Zahid*<sup>c</sup>, *Jin Wang*<sup>d</sup>, *Michael S. H. Boutilier*<sup>c</sup>, *Emmanuel A. Ho*<sup>d,e</sup>, *Arghya Paul*<sup>a,b,c\*</sup>

<sup>a</sup> School of Biomedical Engineering, The University of Western Ontario, London, ON N6A 5B9, Canada.

<sup>b</sup> Department of Chemistry, The University of Western Ontario, London, ON N6A 5B9, Canada.

<sup>c</sup> Department of Chemical and Biochemical Engineering, The University of Western Ontario, London, ON N6A 5B9, Canada.

<sup>d</sup> School of Pharmacy, Faculty of Science, University of Waterloo, 10 Victoria St S, Kitchener, ON N2G 1C5, Canada.

<sup>e</sup> Waterloo Institute for Nanotechnology, University of Waterloo, 200 University Ave West, Waterloo, ON N2L3G1

\* Email: [arghya.paul@uwo.ca](mailto:arghya.paul@uwo.ca)

## **ABSTRACT**

Current nanostructured biomaterials-based drug delivery vehicles for bone regeneration applications often show sub-optimal cellular uptake and inferior drug loading. To overcome these challenges, we have developed a biomimetic cell-derived nanoparticle (CDN) loaded with the FDA-approved small molecule therapeutic Dexamethasone, to induce osteogenic differentiation in human adipose-derived stem cells. The drug-loaded CDNs were cytocompatible, maintained hydrodynamic stability with uniform spherical shape and size, exhibited high percentage drug loading, along with rapid cellular uptake and stem cell differentiation. These results demonstrate for the first time the preparation of Dexamethasone-loaded CDNs capable of directing stem cell fate for advanced bone regeneration applications.

**KEYWORDS:** nanoparticles, drug delivery, bone repair, nanomedicine, regenerative medicine.

Occurrence of critical bone defects - caused by severe injuries, trauma, tumor resection or infections - has increased significantly over the past several years.<sup>1,2</sup> Although bone has regenerative capacity, the repair of these bone injuries and defects in a timely and appropriate manner requires pharmaceutical intervention<sup>3,4</sup>. Pharmaceutical drug molecules play an important role in regulating cellular function and influencing intercellular communication through the regulation of signaling pathways involved in bone remodeling<sup>5</sup>. Several drug molecules, such as growth factors, peptides, small molecule drugs, and genetic material, have been tested to heal bone fractures<sup>6,7</sup>. However, administering osteoinductive molecules in the absence of a carrier is challenging because of poor targeting efficiency, short half-life, and undesirable degradation<sup>8</sup>. To counter these disadvantages, nanostructured particles have been widely exploited as carriers for drug delivery<sup>9</sup>. Both inorganic (e.g. cerium oxide and tungsten disulfide nanoparticles), organic (e.g. liposomes) and biological nanoparticles (e.g. exosomes, virus like nanoparticles) have shown promising abilities in this regard<sup>10-13</sup>. Despite the progress, reproducible strategies to treat bone injuries using nanoparticles remain elusive under clinical settings. Some of the common challenges of the conventional nanoparticle-based drug delivery systems include toxicity and biocompatibility-related issues, inferior drug-loading, poor cellular uptake capacity, and early clearance<sup>6,14</sup>. Cell-derived nanoparticles (CDN), produced from cell membranes, are an emerging class of biomimetic nanoparticles that offer several advantages, including greater biocompatibility and increased cellular uptake capacity<sup>15</sup>. Further, CDN are multicomponent particles made up of cytocompatible cell membrane-based components, such as lipids, proteins, and carbohydrates. The primary goal of this research was to provide a proof of concept to show the potential of drug-loaded CDN to induce differentiation of human adipose-derived stem/stromal cells (ASCs) for

enhanced stem cell therapy. Herein, CDN were used to encapsulate dexamethasone (Dex), an FDA approved glucocorticoid drug <sup>16</sup>, which promoted osteogenic differentiation in ASCs (**Figure 1**).

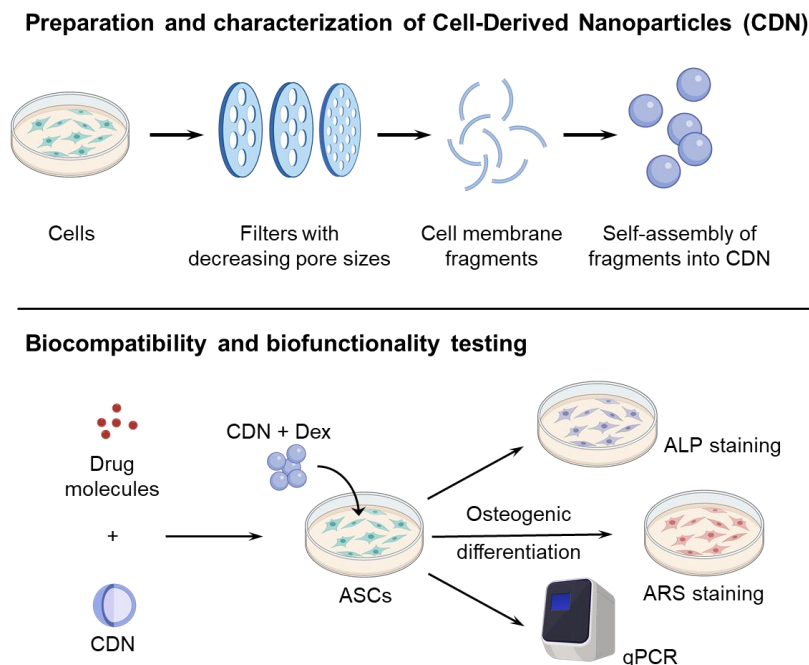


**Figure 1.** Schematic showing the preparation steps of CDN by cell membrane fragmentation and shearing, followed by differentiation of stem cells (ASCs) using CDN loaded with drug (Dex).

To prepare cell-derived nanoparticles, we used human embryonic kidney (HEK) 293 cell line as the source material and centrifugation-based cell shearing technique <sup>17</sup>. We used HEK 293 cell line because of its low maintenance, easy scale up and biomanufacturing process, and wide use in cell biology and biopharmaceutical sectors. At first, the cells were passed through a series of filter membranes with decreasing pore sizes in each subsequent step (**Figure 2A**). HEK293 cells were selected because of their rapid growth and low to minimal variability in different batches. However, the adapted method can be applied to other cells of interest to explore the potential of CDN with similar physical characteristics <sup>18</sup>. Furthermore, cell membranes can self-assemble

spontaneously due to the presence of hydrophobic interactions between the phospholipid groups, thus forming vesicles/particles which entrap the drug molecules <sup>19</sup>. These particles were then passed through a protein concentrator of 10 kDa molecular weight cut off to remove the unloaded Dex. Dex molecules are small, with a size less than 1000 Da, and hence readily passed through the concentrator. The final protein concentration of the CDN was found to be  $4.59 \pm 1.3$  mg/mL (**Figure 2B**). Further, the DNA concentration was found to be  $1933.23 \pm 263.07$  ng/ $\mu$ L and showed a reduction of  $86.2 \pm 5.11\%$  compared to the lysate indicating the removal of a significant quantity of DNA using this method (**Figure 2C**). The shape of the CDN was confirmed by transmission electron microscope (TEM; 420 Transmission Microscope, Philips) and atomic force microscope (AFM; Asylum Research, Oxford Instruments). TEM images of CDN and CDN Dex samples showed that the particles were uniformly spherical in shape and well dispersed (**Figure 2D**). Similar results were seen in the AFM images (**Figure S1**).

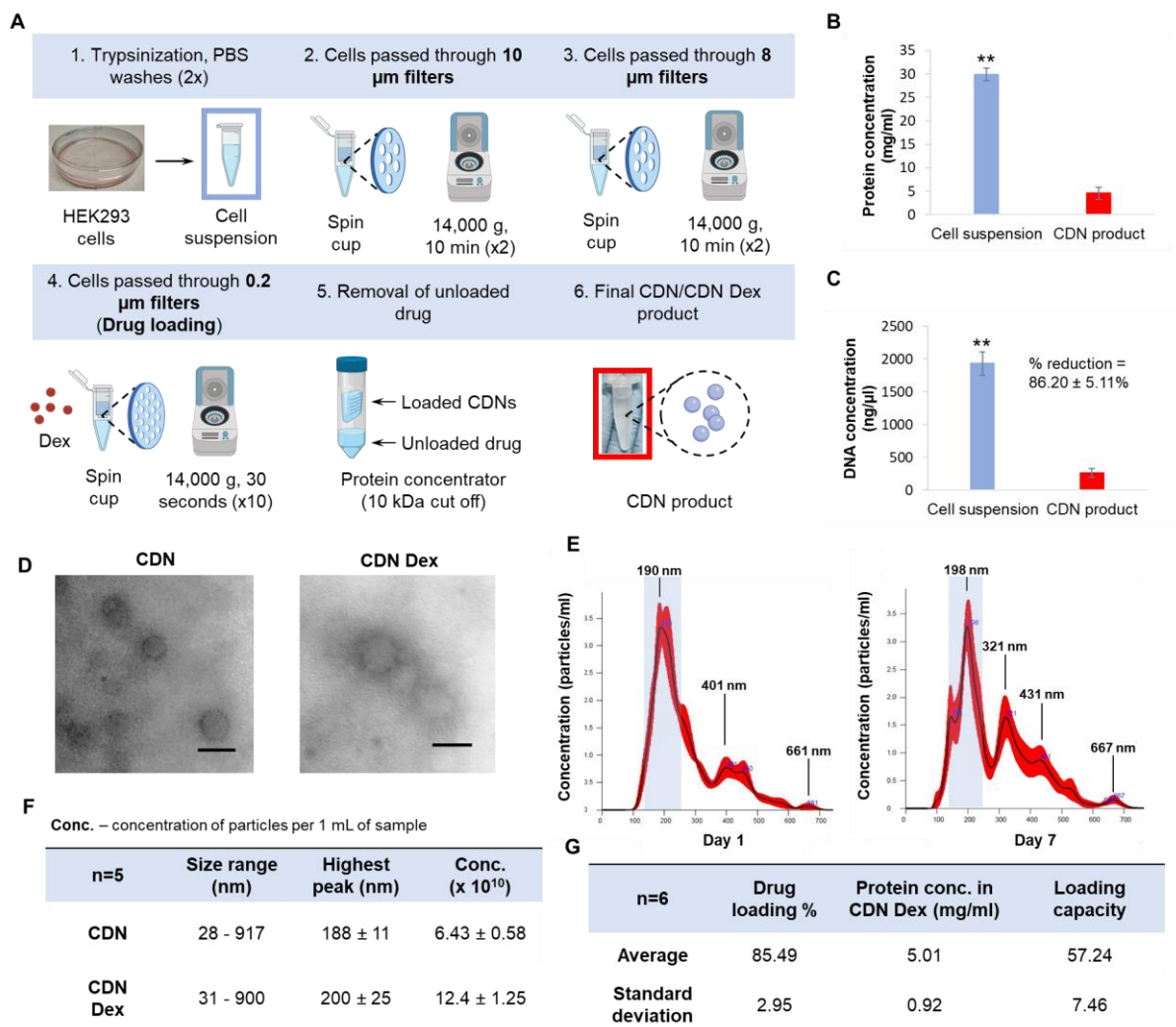


**Figure 2. Preparation and characterization of CDN.** A) Illustration shows the steps involved with the preparation and drug loading of CDN. B) Protein concentrations of the samples at the first and last stages of the preparation process were measured. Results are shown as mean  $\pm$  S.D. (n=3). C) Similarly, DNA concentrations were also measured. D) Depicts the TEM images of the CDN and CDN Dex samples. Particles were uniformly circular and appear to be dispersed. (Scale bar = 100 nm). E) Size vs concentration graph obtained using nanoparticle tracking analysis shows the distribution of nanoparticle sizes in Day 1 and 7 CDN Dex samples. The size of the particles with the highest peaks were around 200 nm and a high concentration of particles was obtained for each sample. F) Table shows the size of the highest peaks and the concentration of particles per 1 mL of sample. G) Table shows the percentage off drug (Dex) loading into CDN with protein concentration in CDN Dex and the final loading capacity of the CDN. Results are shown as mean  $\pm$  S.D. (n=3).

Next, the drug loaded CDN Dex and the unloaded CDN were characterized in terms of size using NanoSight NS300 based on nanoparticle tracking analysis. Individual samples of CDN Dex and



CDN were prepared, and their sizes were analyzed on Days 1 and 7. The graphs generated with particle size vs particle concentration, obtained from NanoSight NS300, showed that there was a distribution of differently sized particles in each of the samples tested, with graphs of the Day 1 and Day 7 samples shown in **Figure 2E**. The maximum number of particles were between the size range of 180-230 nm, shown by the highest peaks in the graphs. Furthermore, size characterization of the different samples of CDN prepared on different days, and stored at 4 °C, showed that the sizes of the CDN remained constant over time. This agrees with previous work which showed that CDN were stable and maintained their sizes for up to 3 weeks<sup>17</sup>. Hence, CDN are stable in PBS indicating the possibility of manageable and ideal storage conditions in the event of large-scale production.

In addition, the particle concentration was ranged from  $6.43 \times 10^{10}$  to  $12.4 \times 10^{10}$  particles per mL of the sample (**Figure 2F**) indicating that a high concentration of differently sized CDN can be obtained. Studies have shown that nanoparticles with sizes between 20 – 200 nm are ideal as delivery vehicles due to their ability to be internalized effectively by cells using different endocytosis pathways<sup>20,21</sup>. While all the particles obtained using this preparation method do not fall in this range, most of the particles do, as seen by the highest intensity peaks, which would promote their internalization. On the other hand, Jiang et al. have shown that increasing or decreasing the initial number of cells used for CDN preparation can have an effect on the size of the particles<sup>18</sup>. This, in combination with an appropriate size exclusion column, can be used as a method to vary the final size of the CDN for different applications.

Next, we determined the amount Dex that was encapsulated inside the CDN. It was found that an average of  $85.49 \pm 2.95\%$  of the total Dex (2 mg) added to the solution was loaded into the CDN

as shown in **Figure 2G**. Therefore, the drug loading percentage indicates that CDN can encapsulate Dex with high loading efficiency.

Further, we wanted to determine the surface-protein characteristics of the synthesized CDN using SDS-PAGE and western blotting. Cells express several proteins and receptors on their surface and on the cell membranes which are responsible for mediating the interaction of the cells with other cells and molecules in the microenvironment surrounding them and within them <sup>17,22</sup>. When CDN are prepared using the membrane fragmentation and cell shearing approach, these surface proteins and membrane proteins are carried over to the nanoparticles formed <sup>17,18</sup>. The presence of one such membrane protein, Caveolin-1, on the CDN was determined using SDS-PAGE and western blotting. Caveolin-1 has a molecular weight of 22 kDa, and is the primary protein present on caveolae, which are invaginations present on the plasma membrane <sup>23,24</sup>. For the western blot, 20  $\mu$ g and 40  $\mu$ g of the CDN Dex and the CDN samples were used. From the blot obtained (**Figure S2**), clear bands can be seen at a molecular weight of 22 kDa proving the presence of Caveolin-1 in both CDN Dex and CDN samples. This indicated that the preparation process and the presence of Dex did not influence the membrane proteins of the cell membrane. Similar results were seen in a study by Ilahibaks et al. who showed the presence of a surface protein, flotillin-1, in CDNs prepared from HEK293 cells using a similar method <sup>25</sup>.

The cytocompatibility of the CDN *in vitro* was tested by treating ASCs with different amounts of CDN. The doses of CDN used were 42 ng, 420 ng, and 4200 ng. The amounts used correspond to the average amounts of CDN used for the osteogenic differentiation of stem cells in the subsequent experiments. Cell viability of ASCs treated with the 3 doses of CDN for 24 hours were tested qualitatively using a live cell staining to show the absence of cytotoxicity. Fluorescence and

brightfield images taken after 24 hours show the presence of viable cells in the control and experimental groups (**Figure 3A**), indicating the absence of intrinsic cytotoxicity of the CDN.

Cytocompatibility of CDN was further confirmed by quantifying the cell proliferation rate using an MTS assay on ASCs treated with different doses of CDN. From **Figure 3B**, it was seen that the control and all the experimental groups showed no significant difference in cell proliferation after 24 hours. A significant difference in cell proliferation was observed between the CDN medium-normal media and the CDN high-normal media groups after 48 hours, however, the cell proliferation normalized after 72 hours. The absence of significant difference in cell proliferation after 72 hours indicates that CDN had no adverse or cytotoxic effects on the growth of ASCs.

The presence of pro-inflammatory responses in THP-1 (human leukemia monocytic cell line) derived macrophages when exposed to different doses of CDN for 24 hours were tested using a TNF- $\alpha$  ELISA kit (R&D Systems). The negative control used for this experiment was macrophages in basal media (no treatment) and the positive control was macrophages treated with lipopolysaccharide (LPS), which is known to induce the production of pro-inflammatory cytokines in macrophages. The presence of TNF- $\alpha$ , a pro-inflammatory cytokine produced in response to infection, in the supernatant after 24 hours was tested<sup>26</sup>. It was found that the experimental groups treated with different doses of CDN showed no significant difference in TNF- $\alpha$  production compared to the negative control (**Figure 3C**), while the LPS group showed significantly high TNF- $\alpha$  concentration in the supernatant. This further proves that the CDN are biocompatible and do not induce the production of pro-inflammatory cytokines.

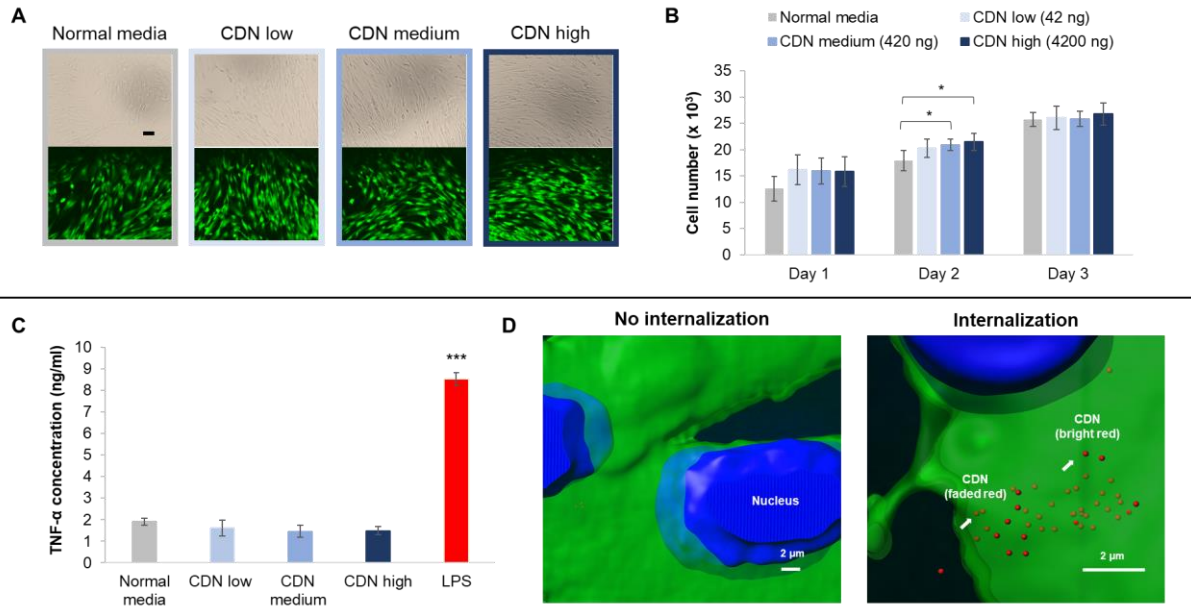


**Figure 3. Cytocompatibility analysis and internalization of CDN.** A) Brightfield and fluorescence images of ASCs treated with different concentrations of CDN for 24 hours and stained with Calcein AM. Viable cells were observed in all the treated groups. (Scale bar = 100  $\mu$ m). B) MTS cell proliferation assay shows the cell numbers of ASCs treated with different doses of CDN for 24, 48, and 72 hours. No significant difference in cell proliferation between the groups was observed after 72 hours. Results are shown as mean  $\pm$  S.D. (n=5). C) Cytokine assay quantifying the secretion of TNF- $\alpha$  by macrophages after treatment with different doses of CDN for 24 hours. No significant difference in TNF- $\alpha$  secretion was observed in the experimental groups when compared to the negative control. Results are reported as mean  $\pm$  S.D. (n=3). D) Internalization of CDN by ASCs. The image on the left does not have any CDN, and the image on the right has CDN that are internalized (faded red) and CDN that are not internalized (bright red). (Scale bars = 2  $\mu$ m). (\*= $p < 0.05$ , \*\*\*= $p < 0.001$ ).

The internalization of the CDN by ASCs was tested by staining the CDN with a lipophilic fluorescent membrane dye, Dil stain (ThermoFisher Scientific). The obtained fluorescent images were analyzed using the Imaris software, which resolves the diffracted light from individual points, to visualize the presence of particles inside and outside the cells. The analyzed image on the right, in **Figure 3D**, shows the presence of bright and faded red spots, where the bright spots indicate particles outside the cell and the faded red spots indicate particles inside the cells. The image on the left does not have any red spots indicating the absence of CDN. These images indicate that the

CDN were internalized by the stem cells. This is similar to results seen in literature that tested the uptake of CDN by other cell types <sup>25</sup>. Furthermore, we tested the internalization of CDN-Dex by ASCs, MC3T3s, HUVECs, and ATDC-5s as a function of time to show the versatility and efficiency of the CDN-based delivery vehicle (**Figures S3 and S4**). The ability to be internalized by cells is an important property of nanoparticles to enable efficient delivery of its payload. It can allow for the nanoparticle to deliver membrane impermeable drugs, hydrophobic drugs, and drugs with low bioavailability <sup>18</sup>.

After confirming the cytocompatibility of CDN, we tested the biofunctionality of CDN loaded with Dex in promoting the osteogenic differentiation of ASCs (**Figure 4A**). The first step of this process was to check for the presence of alkaline phosphatase (ALP) activity, which is an indicator that the fate of the ASCs is progressing towards the osteoblast lineage.

ALP activity was checked on Day 7 and Day 14 using a chromogenic solution that forms a purple substrate in the presence of ALP as shown in **Figure 4B(i)**. It was seen that ALP expression was significantly higher in the CDN Dex and the Dex groups on both days when compared to the control and CDN groups. Moreover, there was no significant difference between the ALP activity in the CDN Dex and Dex groups indicating that the CDN Dex shows comparable activity to the positive control group (**Figure 4C**).

The presence of osteogenic differentiation was further confirmed by detecting the presence of calcium deposits, an indicator that matrix mineralization by osteoblast cells is occurring. This was done using alizarin red S (ARS) staining on Day 14 and Day 21. It was seen that both CDN Dex and Dex showed significantly higher mineral deposition compared to the control and CDN groups as shown in **Figure 4B(ii)**. This trend was seen on both Day 7 and Day 14 indicating that the CDN

Dex group consistently shows higher osteoinductive potential. Furthermore, between the CDN Dex and Dex groups, the CDN Dex group shows higher mineralization (**Figure 4C**). This is an indicator that CDN Dex could be performing better than the free Dex, showing that encapsulation within the CDN can increase the efficiency of the drug molecule. This could be a result of the internalization of the particle, leading to the direct delivery of the drugs to the cells. Further analysis of the internalization pathways and markers is necessary to provide more evidence and insight to this observation.

The results of the ARS staining were further confirmed by running a qPCR analysis to test the expression of 3 osteogenic genes: *RUNX2*, *OCN*, and *OPN* on Day 21. *RUNX2* was expressed in all the experimental groups on Day 21, with the CDN Dex group showing a significant increase in expression compared to the control group (**Figure 4D**). Furthermore, there was no significant difference in expression levels between CDN Dex and Dex, and the CDN and control. This indicates that the CDN Dex and Dex groups are showing comparable osteoinductive activities. A similar trend was seen in the expression of *OPN* and *OCN* on Day 21, where there was a significant increase in the expression of these markers in the CDN Dex group when compared to the control group. This further supports the previous results, confirming that CDN Dex can effectively deliver Dex and promote the osteogenic differentiation of ASCs.

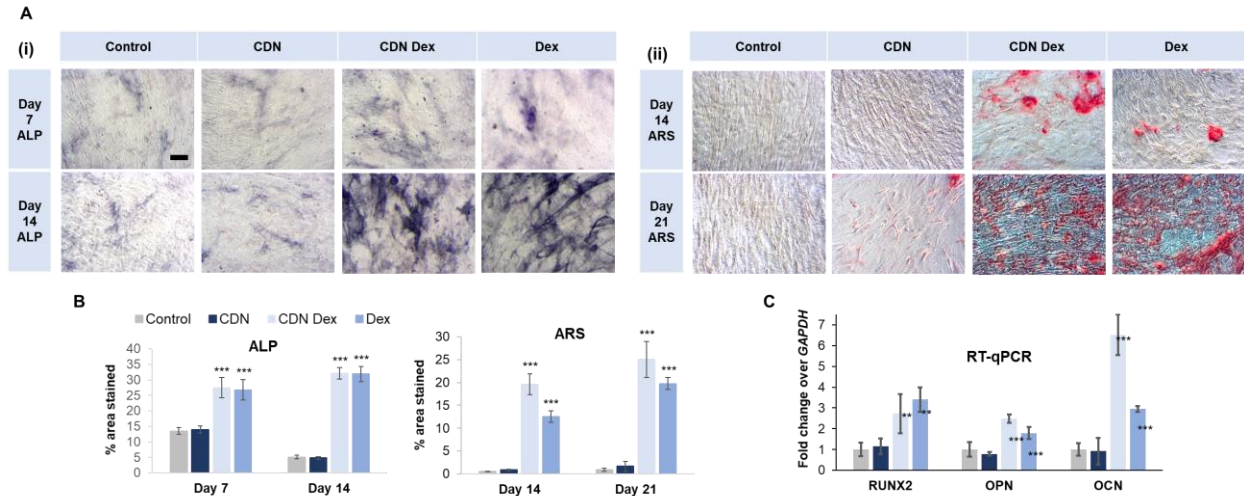


**Figure 4. Determination of alkaline phosphatase activity, calcium deposition and expression of osteogenic genes in ASCs treated with CDN.** A) (i) ALP activity in ASCs treated with CDN Dex (10  $\mu$ M), Dex (10  $\mu$ M), CDN, and control on Days 7 and 14. ALP activity was observed in CDN Dex and Dex groups on both days. (Scale bar = 100  $\mu$ m). (ii) Next, ARS staining to detect calcium deposition in ASCs treated with CDN Dex (10  $\mu$ M), Dex (10  $\mu$ M), CDN, and control on Days 14 and 21. Mineral (calcium) deposits were found in both CDN Dex and Dex groups on Days 14 and 21. (Scale bar = 100  $\mu$ m). B) Later, the images of ALP and ARS stains were quantified using the ImageJ software. CDN Dex and Dex groups showed significant increase in ALP activity compared to the CDN and control groups. Similarly, in case of the ARS stain, CDN Dex and Dex groups showed significant increase in mineralization compared to the CDN and control groups. Results are shown as mean  $\pm$  S.D. (n=3). (\*\*\*=p<0.001). C) RT-qPCR analysis was used to determine the expression of osteogenic markers. CDN Dex showed significant increase in RUNX2, OPN, and OCN expression compared to the control group. Results are reported as mean  $\pm$  S.D. (n=3) (\*\*=p<0.01, \*\*\*=p<0.001).

In summary, here we report the development of a nanoengineered, biomimetic, drug delivery system using HEK 293 cell-derived nanoparticles. These particles are highly non-cytotoxic, exhibit increased cellular uptake compared to free drugs, are multicomponent particles (made of lipids, proteins, and carbohydrates) that mimic cells, and have been shown to efficiently promote osteogenic differentiation of ASCs when loaded with Dexamethasone. While this work establishes the potential of CDN as a new class of nanoparticle for drug delivery and tissue repair applications, further optimization of the CDN preparation process is necessary to overcome its current limitations, such as the presence of trace amounts of genomic DNA in the developed nanocarriers.

Although we show that there is a reduction in the DNA content by ~87%, the safe use of CDN for a wide range of applications requires the complete removal of genetic material or proof of the absence of adverse reactions <sup>27,28</sup>. This will prevent undesired immunogenicity due to the CDN. Furthermore, we need to systematically study the cellular uptake pathways and nano-bio interactions at target site to facilitate further therapeutic advancements in this area. Additionally, similar cell membrane-derived nanocarriers have been successfully applied *in vivo* for various biomedical applications, including cancer therapy <sup>29</sup>, vascular disease treatment <sup>30</sup>, cartilage regeneration <sup>31</sup>, among others [15]. However, to the best of our knowledge, CDNs are yet to be used in the treatment of osteoporosis, osteoarthritis, and other severe bone defect-based complications. Therefore, in our future work, we propose to demonstrate the osteogenic potential of the developed CDN-based bone regenerative platform using *in vivo* calvarial, femoral, and ulnar defect models. Lastly, biomaterial-based scaffolds and grafts have shown promising results for bone regeneration <sup>32</sup>. It can be envisioned that such grafts loaded with CDN may enhance their overall translational potential. **Figure 5** displays some therapeutics delivery strategies and probable biomedical applications of the CDN in combination with polymeric scaffolds. Future investigations should include the preparation of CDNs with injectable hydrogel-based scaffolds for non-load bearing bone defects as well as CDN/hydrogel coating agents to biofunctionalize existing commercial orthopedic implants.



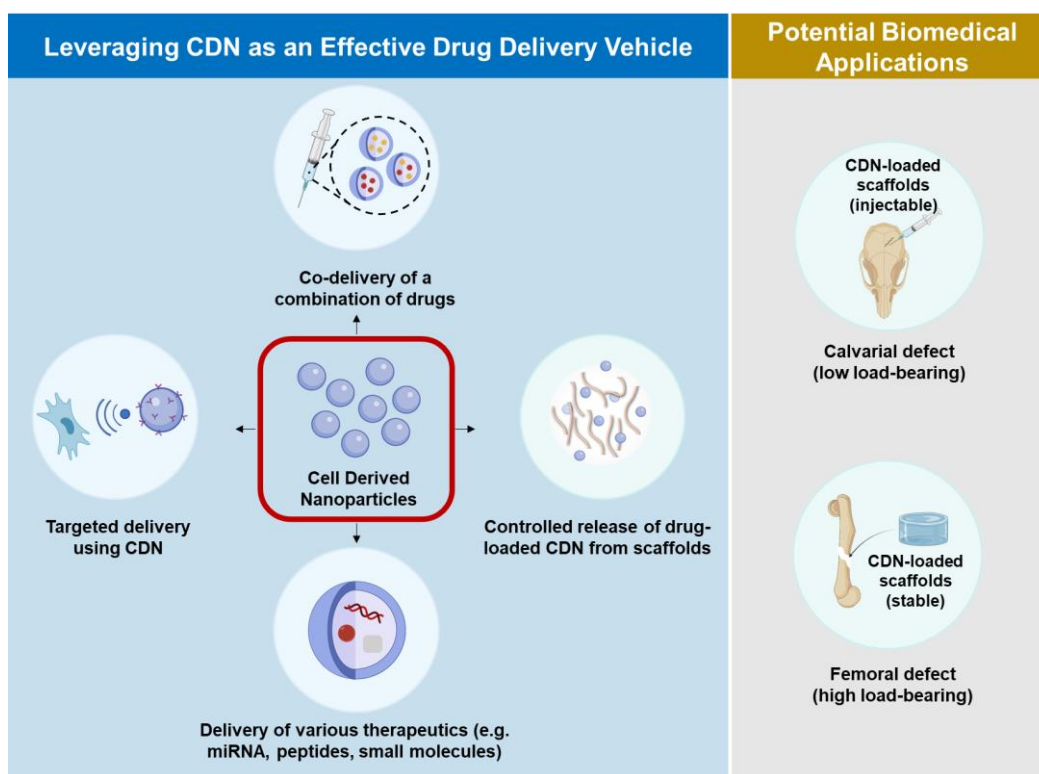


**Figure 5. Proposed delivery approaches and osteogenic applications of the developed CDN.** The synthesized CDN may deliver small or large molecules and can also be designed specifically for targeted therapy. Additionally, CDN may be delivered with polymeric scaffolds, such as hydrogels, electrospun fibers, among others to further sustain the release of the encapsulated therapeutics. The illustration also highlights the potential of CDN combined with injectable or scaffold-based platforms to enhance bone regeneration.

### Supporting Information.

Additional experimental details and materials and methods.

### AUTHOR INFORMATION

#### Corresponding Author

Arghya Paul - arghya.paul@uwo.ca

## **Author Contributions**

The manuscript was written through contributions of all authors. All authors have given approval to the final version of the manuscript.

## **ACKNOWLEDGMENT**

A.P. would like to gratefully acknowledge the funding and supports from Canada Research Chairs Program of the Natural Sciences and Engineering Research Council (NSERC) of Canada, NSERC Discovery Grant, NSERC Discovery Accelerator Supplements (DAS), New Frontiers in Research Fund (NFRF) - Exploration Stream, Early Research Award (ERA) from Province of Ontario, Wolfe-Western Fellowship At-Large for Outstanding Newly Recruited Research Scholar, The Centre for Advanced Materials and Biomaterials Research (CAMBR) Seed Grant, and Western Strategic Support-CIHR Seed Grant. The authors would like to acknowledge Reza Khazaei and Karen Nygard from Biotron Integrated Microscopy Facility for their help with TEM, fluorescence microscopy, and image analysis. The authors would like to thank Prof. Subrata Chakrabarti and Prof. Francis Feng for allowing access to their lab instruments, and Prof. Lauren Flynn for providing THP-1 cells for the experiments. The authors declare that there is no conflict of interest regarding the publication of this article. The authors would like to acknowledge BioRender, some of the images and illustrations were created with BioRender.com.

## **ABBREVIATIONS**

AFM            Atomic force microscopy

ALP            Alkaline phosphatase

ANOVA        Analysis of variance

ARS	Alizarin red S
CDN	Cell derived nanoparticles
DAPI	4',6-diamidino-2-phenylindole
Dex	Dexamethasone
DiI	1,1'-Dioctadecyl-3,3',3'-Tetramethylindocarbocyanine Perchlorate
DNA	Deoxyribonucleic acid
FBS	Fetal bovine serum
hADSC	Human adipose-derived stem cells
HEK293	Human embryonic kidney 293 cells
LPS	Lipopolysaccharide
PBS	Phosphate buffered saline
RNA	Ribonucleic acid
RT-qPCR	Reverse transcription quantitative polymerase chain reaction
RUNX2	Runt-related transcription factor 2
SDS-PAGE	Sodium dodecyl sulphate-polyacrylamide gel electrophoresis
TEM	Transmission electron microscopy
THP1	Human acute monocyte leukaemia cell line
TNF- $\alpha$	Tumour necrosis factor alpha

## References

- (1) Holkar, K.; Vaidya, A.; Pethe, P.; Kale, V.; Ingavle, G. Biomaterials and Extracellular Vesicles in Cell-Free Therapy for Bone Repair and Regeneration: Future Line of Treatment in Regenerative Medicine. *Materialia*. **2020**, *12*, 100736,

<https://doi.org/10.1016/j.mtla.2020.100736>.

- (2) Ansari, M. Bone Tissue Regeneration: Biology, Strategies and Interface Studies. *Prog in Biomaterials*. **2019**, 8, 223–237, <https://doi.org/10.1007/s40204-019-00125-z>.
- (3) Lin, H.; Sohn, J.; Shen, H.; Langhans, M. T.; Tuan, R. S. Bone Marrow Mesenchymal Stem Cells: Aging and Tissue Engineering Applications to Enhance Bone Healing. *Biomaterials* **2019**, 203, 96-110, <https://doi.org/10.1016/j.biomaterials.2018.06.026>.
- (4) Majidinia, M.; Sadeghpour, A.; Yousefi, B. The Roles of Signaling Pathways in Bone Repair and Regeneration. *J. Cell. Physiol.* **2018**, 233(4), 2937-2948, <https://doi.org/10.1002/jcp.26042>.
- (5) Kim, S.; Lee, S.; Kim, K. Bone Tissue Engineering Strategies in Co-Delivery of Bone Morphogenetic Protein-2 and Biochemical Signaling Factors. *Adv. Exp. Med. Biol.* **2018**, 1078, 233-244, [https://doi.org/10.1007/978-981-13-0950-2\\_12](https://doi.org/10.1007/978-981-13-0950-2_12).
- (6) Rothe, R.; Hauser, S.; Neuber, C.; Laube, M.; Schulze, S.; Rammelt, S.; Pietzsch, J. Adjuvant Drug-Assisted Bone Healing: Advances and Challenges in Drug Delivery Approaches. *Pharmaceutics*. **2020**, 12(5), 428, <https://doi.org/10.3390/pharmaceutics12050428>.
- (7) Eivazzadeh-Keihan, R.; Chenab, K. K.; Taheri-Ledari, R.; Mosafer, J.; Hashemi, S. M.; Mokhtarzadeh, A.; Maleki, A.; Hamblin, M. R. Recent Advances in the Application of Mesoporous Silica-Based Nanomaterials for Bone Tissue Engineering. *Mater. Sci. Eng. C*. **2020**, 107, 110267, <https://doi.org/10.1016/j.msec.2019.110267>.
- (8) Cheng, H.; Chawla, A.; Yang, Y.; Li, Y.; Zhang, J.; Jang, H. L.; Khademhosseini, A. Development of Nanomaterials for Bone-Targeted Drug Delivery. *Drug. Discov. Today*. **2017**, 22(9), 1336-1350, <https://doi.org/10.1016/j.drudis.2017.04.021>.

- (9) Martínez-López, A. L.; Pangua, C.; Reboredo, C.; Campión, R.; Morales-Gracia, J.; Irache, J. M. Protein-Based Nanoparticles for Drug Delivery Purposes. *Int. J. Pharm.* **2020**, 581, 119289, <https://doi.org/10.1016/j.ijpharm.2020.119289>.
- (10) Lombardo, D.; Kiselev, M. A.; Caccamo, M. T. Smart Nanoparticles for Drug Delivery Application: Development of Versatile Nanocarrier Platforms in Biotechnology and Nanomedicine. *J. Nanomater.* **2019**, 2019, 1-26, <https://doi.org/10.1155/2019/3702518>.
- (11) Augustine, R.; Zahid, A. A.; Hasan, A.; Dalvi, Y. B.; Jacob, J. Cerium Oxide Nanoparticle-Loaded Gelatin Methacryloyl Hydrogel Wound-Healing Patch with Free Radical Scavenging Activity. *ACS Biomater. Sci. Eng.* **2021**, 7(1), 279–290, <https://doi.org/10.1021/acsbiomaterials.0c01138>.
- (12) Basu, S.; Chakraborty, A.; Alkiswani, A. R. I.; Shamiya, Y.; Paul, A. Investigation of a 2D WS<sub>2</sub>nanosheet-Reinforced Tough DNA Hydrogel as a Biomedical Scaffold: Preparation and: In Vitro Characterization. *Mater. Adv.* **2022**, 3(2), 946–952, <https://doi.org/10.1039/d1ma00897h>.
- (13) Kulkarni, A. A.; Vijaykumar, V. E.; Natarajan, S. K.; Sengupta, S.; Sabbiseti, V. S. Sustained Inhibition of CMET-VEGFR2 Signaling Using Liposome-Mediated Delivery Increases Efficacy and Reduces Toxicity in Kidney Cancer. *Nanomedicine*. **2016**, 12(7), 1853-1861, <https://doi.org/10.1016/j.nano.2016.04.002>.
- (14) Zahid, A. A.; Chakraborty, A.; Shamiya, Y.; Ravi, S. P.; Paul, A. Leveraging the Advancements in Functional Biomaterials and Scaffold Fabrication Technologies for Chronic Wound Healing Applications. *Mater. Horizons*. **2022**, 9, 1850-1865, <https://doi.org/10.1039/D2MH00115B>
- (15) Le, Q. V.; Lee, J.; Lee, H.; Shim, G.; Oh, Y. K. Cell Membrane-Derived Vesicles for

- Delivery of Therapeutic Agents. *Acta. Pharm. Sin. B.* **2021**, 11(8), 2096-2113, <https://doi.org/10.1016/j.apsb.2021.01.020>.
- (16) Yuasa, M.; Yamada, T.; Taniyama, T.; Masaoka, T.; Xuetao, W.; Yoshii, T.; Horie, M.; Yasuda, H.; Uemura, T.; Okawa, A.; Sotome, S. Dexamethasone Enhances Osteogenic Differentiation of Bone Marrow-and Muscle-Derived Stromal Cells and Augments Ectopic Bone Formation Induced by Bone Morphogenetic Protein-2. *PLoS. One.* **2015**, 10(2), e0116462, <https://doi.org/10.1371/journal.pone.0116462>.
- (17) Chakravarti, A. R.; Pacelli, S.; Paul, A. Investigation of Human Adipose Stem Cell-Derived Nanoparticles as a Biomimetic Carrier for Intracellular Drug Delivery. *Nanoscale.* **2020**, 12(47), 24273–24284, <https://doi.org/10.1039/d0nr06571d>.
- (18) Goh, W. J.; Zou, S.; Ong, W. Y.; Torta, F.; Alexandra, A. F.; Schiffelers, R. M.; Storm, G.; Wang, J. W.; Czarny, B.; Pastorin, G. Bioinspired Cell-Derived Nanovesicles versus Exosomes as Drug Delivery Systems: A Cost-Effective Alternative. *Sci. Rep.* **2017**, 7, 14322, <https://doi.org/10.1038/s41598-017-14725-x>.
- (19) Nicolson, G. L. The Fluid - Mosaic Model of Membrane Structure: Still Relevant to Understanding the Structure, Function and Dynamics of Biological Membranes after More than 40 Years. *Biochim. Biophys. Acta. Biomembr.* **2014**, 1838(6), 1451-1466, <https://doi.org/10.1016/j.bbamem.2013.10.019>.
- (20) Augustine, R.; Hasan, A.; Primavera, R.; Wilson, R. J.; Thakor, A. S.; Kevadiya, B. D. Cellular Uptake and Retention of Nanoparticles: Insights on Particle Properties and Interaction with Cellular Components. *Mater. Today. Commun.* **2020**, 25, 101692, <https://doi.org/10.1016/j.mtcomm.2020.101692>.
- (21) Foroozandeh, P.; Aziz, A. A. Insight into Cellular Uptake and Intracellular Trafficking of

- Nanoparticles. *Nanoscale. Res. Lett.* 2018, 13, 339, <https://doi.org/10.1186/s11671-018-2728-6>.
- (22) Pacelli, S.; Chakravarti, A. R.; Modaresi, S.; Subham, S.; Burkey, K.; Kurlbaum, C.; Fang, M.; Neal, C. A.; Mellott, A. J.; Chakraborty, A.; Paul, A. Investigation of Human Adipose-Derived Stem-Cell Behavior Using a Cell-Instructive Polydopamine-Coated Gelatin–Alginate Hydrogel. *J. Biomed. Mater. Res. - Part A* **2021**, 109 (12), 2597–2610, <https://doi.org/10.1002/jbm.a.37253>.
- (23) Han, B.; Tiwari, A.; Kenworthy, A. K. Tagging Strategies Strongly Affect the Fate of Overexpressed Caveolin-1. *Traffic*. **2015**, 16, 417-438, <https://doi.org/10.1111/tra.12254>.
- (24) Quest, A. F. G.; Gutierrez-Pajares, J. L.; Torres, V. A. Caveolin-1: An Ambiguous Partner in Cell Signalling and Cancer. *J. Cell. Mol. Med.* **2008**, 12, 1130-1150, <https://doi.org/10.1111/j.1582-4934.2008.00331.x>.
- (25) Ilaahibaks, N. F.; Lei, Z.; Mol, E. A.; Deshantri, A. K.; Jiang, L.; Schiffelers, R. M.; Vader, P.; Sluijter, J. P. G. Biofabrication of Cell-Derived Nanovesicles: A Potential Alternative to Extracellular Vesicles for Regenerative Medicine. *Cells*. **2019**, 8(12), 1509, <https://doi.org/10.3390/cells8121509>.
- (26) Parameswaran, N.; Patial, S. Tumor Necrosis Factor- $\alpha$  Signaling in Macrophages Narayanan. *Adv. Glob. Chang. Res.* **2010**, 20(2), 87–103, <https://doi.org/10.1615/critreveukargeneexpr.v20.i2.10>.
- (27) Roers, A.; Hiller, B.; Hornung, V. Recognition of Endogenous Nucleic Acids by the Innate Immune System. *Immunity*. **2016**, 44(4), 739-754, <https://doi.org/10.1016/j.immuni.2016.04.002>.
- (28) Guo, S.; Li, H.; Ma, M.; Fu, J.; Dong, Y.; Guo, P. Size, Shape, and Sequence-Dependent

- Immunogenicity of RNA Nanoparticles. *Mol. Ther. - Nucleic Acids* **2017**, *9*, 399-408, <https://doi.org/10.1016/j.omtn.2017.10.010>.
- (29) Ren, H.; Liu, J.; Li, Y.; Wang, H.; Ge, S.; Yuan, A.; Hu, Y.; Wu, J. Oxygen Self-Enriched Nanoparticles Functionalized with Erythrocyte Membranes for Long Circulation and Enhanced Phototherapy. *Acta Biomater.* **2017**, *59*, 269–282, <https://doi.org/10.1016/J.ACTBIO.2017.06.035>.
- (30) Hao, X.; Li, Q.; Wang, H.; Muhammad, K.; Guo, J.; Ren, X.; Shi, C.; Xia, S.; Zhang, W.; Feng, Y. Red-Blood-Cell-Mimetic Gene Delivery Systems for Long Circulation and High Transfection Efficiency in ECs. *J. Mater. Chem. B.* **2018**, *6* (37), 5975–5985, <https://doi.org/10.1039/C8TB01789A>.
- (31) Zhang, X.; Chen, J.; Jiang, Q.; Ding, X.; Li, Y.; Chen, C.; Yang, W.; Chen, S. Highly Biosafe Biomimetic Stem Cell Membrane-Disguised Nanovehicles for Cartilage Regeneration. *J. Mater. Chem. B.* **2020**, *8*(38), 8884–8893, <https://doi.org/10.1039/D0TB01686A>.
- (32) Ceccarelli, G.; Presta, R.; Benedetti, L.; Cusella De Angelis, M. G.; Lupi, S. M.; Rodriguez Y Baena, R. Emerging Perspectives in Scaffold for Tissue Engineering in Oral Surgery. *Stem. Cells. Int.* **2017**, 2017, 1-11, <https://doi.org/10.1155/2017/4585401>.